Chapter V

Some Experimental Investigations on Type-II Chiral Liquid Crystals

5.1 Introduction

Superconductors are classified into two types depending on their response to an external magnetic filed. The response depends on the Ginzburg parameter $\kappa\ (=\lambda/\xi)$ which is the ratio of the penetration depth (λ) of the magnetic field from the surface, to the coherence length, ξ of the order parameter. If $\kappa<1/\sqrt{2}$, the superconductor completely expels the magnetic field (Meissner effect) up to a critical value of the field above which the superconductivity is destroyed and it transforms to a normal metal. Such materials are called type-I superconductors. On the other hand, if $\kappa>1/\sqrt{2}$, the magnetic field penetrates the superconductor in the form of a triangular lattice of quantised magnetic flux tubes giving rise to an intermediate state between the perfect superconductor and the normal metal. This intermediate phase is known as Abrikosov phase. Materials exhibiting this phase are called type-II superconductors.

It was pointed out by de Gennes that like superconductors SmA liquid crystals can also be classified as type-I and type-II smectics depending on their response to bending or twisting stress [1]. In chiral liquid crystals, the screw dislocations are analogous to the flux tubes in superconductors. Such dislocations in liquid crystals can not be arranged in a triangular lattice [2]. Renn and Lubensky proposed an intermediate structure in which the contrary tendencies of smectic-like layering and cholesteric-like twist coexist [2] in highly chiral liquid crystals. This intermediate phase is called the twist grain boundary-A (TGB_A) phase. In this phase, well defined SmA slabs are separated by regularly spaced planar arrays of parallel screw dislocations (the twist grain boundaries). The layer normals of the successive slabs rotate relative to each other by an angle. Goodby et al [3] experimentally discovered this phase in some highly chiral liquid crystals. Later X-ray diffraction and freeze-fracture experiments have confirmed the

predicted structure of the TGB_A phase [4]. A schematic structure of the TGB_A phase is shown in Fig.(5.1).

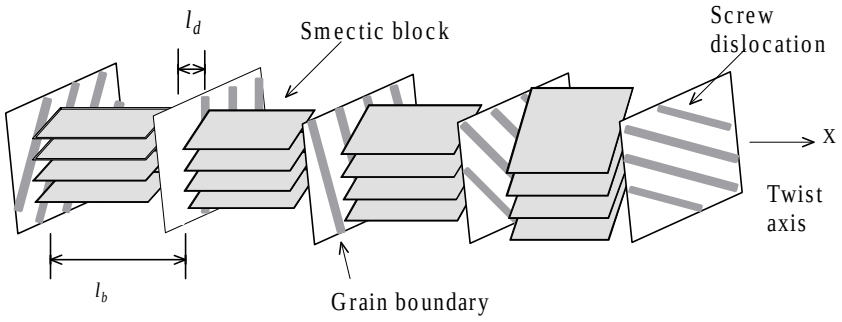

Figure 5.1: Schematic representation of the structure of the TGB_A liquid crystal.

To show the analogy between the Abrikosov phase made of a vortex lattice and TGB_A phase, following Lubensky et al [5] we write the Gibbs free energies for metals in a magnetic field and chiral smectics. The de Gennes free energy density describing nematic to SmA transition is given by [5]

$$F_{deG} = \int d^3x \left[r|\psi|^2 + \frac{g}{2}|\psi|^4 + C_{\|}\left|\frac{\partial \psi}{\partial z}\right|^2 + C_{\perp}\left|(\nabla_{\perp} - iq_0\delta n_{\perp})\psi\right|^2 \right] + F_{el}\,, \tag{5.1}$$

where F_{el} is the energy cost for the distortion of the Frank-director field. ψ is the SmA order parameter as described in equation (1.18) in chapter-I. $r = a(T - T_{AN})$, where T_{AN} is the nematic to smectic transition temperature and a, g are constants. The terms with coefficients $C_{\|}$ and $C_{\perp}$ give the energy cost for creating gradients in the order parameter. The elastic energy F_{el} is given by:

$$F_{el} = \frac{1}{2}\int d^3x \left[K_1(\nabla.\hat{n})^2 + K_2(\hat{n}.\nabla\times\hat{n})^2 + K_3(\hat{n}\times\nabla\times\hat{n})^2\right] \tag{5.2}$$

where K_1, K_2 and K_3 are the elastic constants associated with the splay, twist and bend deformations of the director field. Assuming $C_{\|} = C_{\perp} = C$, and K_1=K_2=K_3=K, equation (5.1) can be written as

$$F_{deG} = \int d^3x \left[r|\psi|^2 + \frac{g}{2}|\psi|^4 + C|(\nabla - iq_0\hat{n})\psi|^2 + K(\nabla.\hat{n})^2 + K(\nabla\times\hat{n})^2 \right]. \qquad (5.3)$$

In case of superconducting metals the Ginzburg-Landau free energy is given by [5]

$$G_{GL} = \int d^3x \left[r|\psi|^2 + \frac{g}{2}|\psi|^4 + \frac{1}{m^*}\left| \left(\hbar\nabla - i\frac{e^*}{c}A \right)\psi \right|^2 + \frac{1}{8\pi\mu}(\nabla\times A)^2 \right] \qquad (5.4)$$

where ψ is superconductor 'gap' complex order parameter, *A* the magnetic vector potential, e^* the electronic charge, *c* the velocity of light, μ the magnetic permeability, $\hbar$ the Planck's constant, m^* the effective mass of the electron. Several superconductor-liquid crystal analogies are seen from equations (5.3) and (5.4). The order parameters in both the systems are complex quantities. In the case of superconductors the order parameter is the Cooper-pair wave function and it is the mass-density wave normal to the layers in the case of SmA. The nematic director $\hat{n}$ is analogous to the magnetic vector potential *A*, and twist or bend $(\nabla\times\hat{n})$ deformations to the magnetic induction ($B = \nabla\times A$). However there is no analogy of the splay deformation in the case of superconductors since $\nabla.A = 0$. Superconductors expel magnetic lines of force; similarly smectic liquid crystals expel twist and bend deformations. These deformations are associated with the change in layer spacing in the SmA phase, which is energetically expensive.

The elastic free energy for the smectic phase is given by [5]

$$\begin{aligned} F &= \frac{1}{2}\int d^3x \left[B(\nabla_{\|}u)^2 + D(\nabla_{\perp}u + \vec{\delta n})^2 \right] \\ &\quad + \frac{1}{2}\int d^3x \left[K_1(\nabla.\hat{n})^2 + K_2(\hat{n}.(\nabla\times\hat{n}))^2 + K_3(\hat{n}\times(\nabla\times\hat{n}))^2 \right] \end{aligned} \qquad (5.5)$$

where *B* measures the energy cost associated with compressing or dilating of the layers. *D* is the elastic constant for director twist or molecular tilt in the layer and *u* is the layer displacement field. With $B = C_{\|}q_0^2|\psi|^2$, $D = C_{\perp}q_0^2|\psi|^2$ the elastic part of equation (5.1) reduces to equation (5.5). From equation (5.5) we can define two lengths $\lambda_2 = \sqrt{K_2/D}$ and $\lambda_3 = \sqrt{K_3/D}$, corresponding to the penetration depths of twist and bend deformations respectively. In smectic liquid crystals the Ginzburg parameter for twist deformation $\kappa_2 = \lambda_2/\xi$, where ξ is the smectic order parameter coherence length. If

$\kappa_2 < 1/\sqrt{2}$, the smectic resists twist deformation until a critical value of the stress at which it melts into a twisted nematic. Such smectic liquid crystals are classified as type-I. In type-II smectics $\kappa_2 > 1/\sqrt{2}$, the twist deformation can penetrate into the smectic in the form of screw dislocations when the stress is increased beyond a critical value. Thus screw dislocations are the liquid crystalline analogue of the magnetic flux tubes in a superconductor.

In case of metals the magnetic field is applied from outside whereas the twist deformation in liquid crystals can be generated intrinsically either by making the molecules chiral or by doping chiral materials in the smectic phase. The term in the Gibbs free energy which favors molecular twist is given by

$$F_{N^*} = -h\int d^3x(\hat{n}.\nabla\times\hat{n}), \tag{5.6}$$

where the magnitude of potential *h* depends on the degree of molecular chirality. A schematic representation of *h*-*T*, phase diagram is shown in Fig.(5.2).

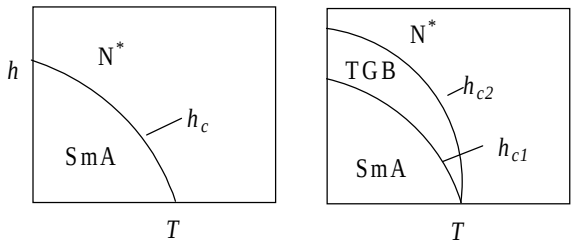

(a) (b)

Figure 5.2: Phase diagram in the *h*-*T* plane. (a) type-I smectics: a first-order transition from the N^* (cholesteric) to the SmA phase at the critical field h_c. (b) type-II smectics: a second order transition from the SmA to the TGB phase at the lower critical field h_{c1} and a second order transition from the TGB to N^* phase at the upper critical field h_{c2} (adapted from ref. [5]).

The TGB_A phase was first observed in some highly *chiral* liquid crystals. Later several authors also reported observations of TGB phases in mixtures of some chiral and nonchiral compounds. The TGB phase with SmC-like blocks (TGB_C) has also been experimentally characterised [6]. The discovery of a new phase called the undulated twist grain boundary smectic-C^* ($UTGB_C^*$) phase was reported in a mixture of a *chiral*

compound 4 - (2-methyl butyl) phenyl 4′ –n –octylbiphenyl – 4 - carboxylate (CE8) and a *nonchiral* compound 2 - cyano 4 – heptylphenyl 4′ – pentyl 4 - biphenyl carboxylate (7(CN)5) from our laboratory by Pramod et al [7]. Several physical studies have been made to characterise this new liquid crystalline phase [8]. Part of the phase diagram is reproduced in Fig.(5.3).

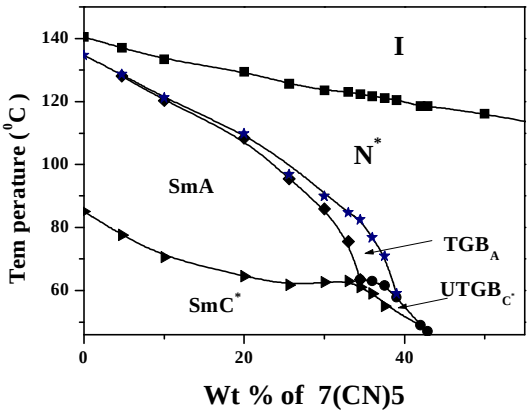

Figure 5.3: Part of the phase diagram containing the TGB phases in binary mixtures of CE8 and 7(CN)5 (adapted from ref.[7]).

It is noticed from the phase diagram that the temperature range of TGB_A phase increases with the concentration of the *nonchiral* compound and above 34 wt% of the latter the $UTGB_C^*$ phase is also induced. The CE8 sample obtained from Merck does not by itself exhibit TGB_A phase, even though recently Wilson et al. [9] have reported that in a highly purified sample it shows the TGB_A phase with a range of ~0.5 ^{0}C. However this is not expected to change the main features of the phase diagram. With decreasing chiral strength the increase in the temperature range of TGB_A phase and also the induction of $UTGB_C^*$ phase is unexpected. Apart from having a sufficiently large chiral strength the material must have a type-II character to exhibit TGB phases [2]. To understand the unusual trend in the phase diagram, we carried out several experimental investigations on a few mixtures of the above compounds. We report the following new experimental results.

(i) optical reflectivity measurements in the cholesteric phase to confirm that the chiral strength of the medium decreases as the concentration of the *nonchiral* compound is increased

(ii) electroclinic measurements in the SmA phase to demonstrate that the tilt elastic constant decreases rapidly with concentration of the nonchiral compound, thus enhancing the type-II character of the mixture

(iii) an irreversible transition from TGB_A phase to SmA phase under the action of a low frequency electric field and

(iv) occurrence of a new type of periodic radial structure in the meniscus region of free standing films. It is suggested that this structure arises from the type-II character of the material.

We will first discuss the theoretical background of the electroclinic effect.

5.2 Electroclinic Effect

Meyer and coworkers discovered in 1975 that SmC liquid crystals made of chiral molecules are ferroelectric [10]. Subsequently many aspects of the ferroelectric phenomena have been studied. A phenomenon related to ferroelectricity is the electroclinic effect inherent in SmA liquid crystals consisting of chiral molecules.

The symmetry elements of an achiral SmC phase are a two-fold axis C_2 perpendicular to the director and lying in the plane of the smectic layers, a mirror plane normal to the two-fold rotation axis and consequently an inversion center *i* (Fig.(5.4)).

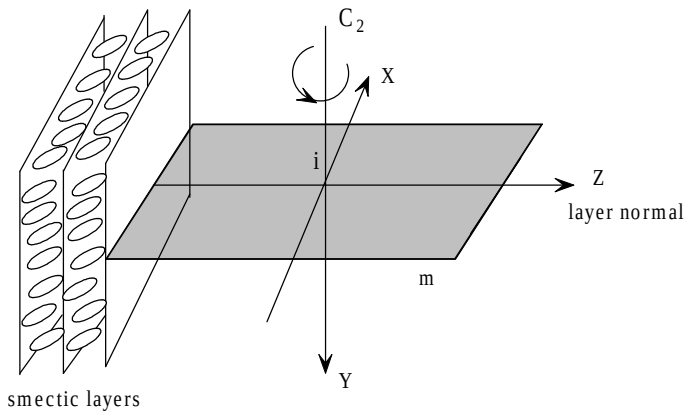

Figure 5.4: Symmetry elements in the SmC phase.

When the SmC liquid crystal is composed of chiral molecules, the mirror plane and thus the inversion center no longer exist and the remaining two-fold axis permits the existence of a permanent electric polarisation parallel to the C_2 axis.

Meyer also argued that a similar symmetry argument leads to an electroclinic effect in the SmA phase composed of chiral molecule [11]. An applied electric field E parallel to the smectic layers couples to the transverse component of the molecular permanent electric dipole ($\vec{p}$). The free rotations of the molecules are hindered about their long axes since $\vec{p}$ is parallel to the applied field. The system has two-fold axis along the electric field as the apolar director is orthogonal to $\vec{p}$. The plane containing the layer normal and $\vec{p}$ is a mirror plane in the nonchiral phase. But in the chiral system, the mirror symmetry of this plane no longer exists. A molecular tilt then can be induced with respect to the layer normal in the orthogonal plane. The electric field induced tilt in the SmA phase composed of chiral molecules is known as the electroclinic effect. There are several reports on electroclinic measurements [11-13]. The temperature variation of electroclinic coefficient can be discussed conveniently using the Landau theory for SmA to SmC* phase transition under the action of an electric field.

In order to obtain the field-induced tilt angle in the SmA phase, we write the free energy expression which includes the electric field. The Landau free energy considering θ as the order parameter [14] is given by

$$f = \frac{1}{2}\alpha\theta^2 + \frac{1}{4}\beta\theta^4 \tag{5.7}$$

where $\alpha = a(T - T_{AC^*})$, $\beta > 0$, $a > 0$ for a second order phase transition. $T_{AC}{}^*$ is the SmA to SmC* transition temperature. The contribution to the free energy due to the externally applied electric field can be written as

$$-\vec{P}.\vec{E} = -kE\theta\cos\phi \tag{5.8}$$

where k is denoted as tilt polarisation coupling constant which is the dipole moment per unit volume for unit tilt angle and ϕ is the angle between the direction of electric field ($\vec{E}$) and the polarisation ($\vec{P}$). ϕ is taken to be zero as the induced polarisation is parallel to the applied field. Using equations (5.7) and (5.8) the free energy can be written as

$$f_0 = \frac{1}{2}\alpha\theta^2 + \frac{1}{4}\beta\theta^4 - kE\theta\,. \tag{5.9}$$

In the SmA phase ($T > T_{AC}^{*}$) as the field induced tilt angle θ is small, then the θ^4 -term can be neglected in comparison with the field-term. Thus equation (5.9) can be written as

$$f_0 = \frac{1}{2}\alpha\theta^2 - kE\theta \,. \tag{5.10}$$

Minimising f_0 with respect to θ we get

$$\theta = \frac{kE}{\alpha} = \frac{kE}{a(T - T_{AC^*})}. \tag{5.11}$$

It is noticed that for small field the induced tilt angle θ is linearly proportional to the applied electric field. The electroclinic coefficient is defined as $e = \theta / E$. From equation (5.11) we get

$$e = \frac{k}{a(T - T_{AC^*})} \tag{5.12}$$

5.3 Experimental

The experimental studies are conducted on binary mixtures consisting of the *chiral* compound 4 - (2 - methyl butyl) phenyl $4'$ - n - octylbiphenyl - 4 - carboxylate (CE8) made by BDH and a *nonchiral* compound 2 - cyano 4 - heptylphenyl $4'$ - pentyl 4- biphenyl carboxylate (7(CN)5) obtained from Merck.

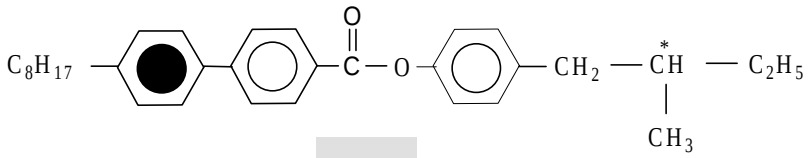

CE8

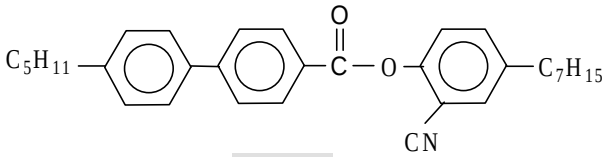

7(CN)5

Figure 5.5: Molecular structure of the two compounds used in the experiments.

CE8 is *chiral* due the presence of the asymmetrically substituted carbon atom. It has the following phase sequence as a function of temperature (in ^{0}C): Cr-67- SmI* -70-SmC* -80.5- SmA -136.5- N* -138.8- BP2- 139.7- BP1- 140.5- I, where BP stands for the blue phases. 7(CN)5 has the phase sequence Cr-45.5-N-102.0-I. The measurements of birefringence and dielectric constants of the compound 7(CN)5 have been reported in chapter–III and chapter–IV respectively.

The mixtures are prepared by weighing precise amounts of the individual compounds in glass cups. The mixtures are heated to the isotropic phase and kept in that phase for a few minutes and stirred with a glass rod to get a uniform concentration. The cells are filled in the isotropic phase and cooled slowly (0.05 ^{0}C/minute) to obtain uniform planar alignment of the molecules in the mesophase.

The electroclinic measurements are made using a standard technique with an A.C. signal at a frequency of 417 Hz and amplitude of 5 volts. The schematic diagram of the experimental setup is shown in Fig.(5.6). The temperature of the cell is controlled by a hotstage (INSTEC HS1) to an accuracy of ~10mK. For the optical and electroclinic measurements, the sample is sandwiched between two ITO coated glass plates separated by spacers of ~5μm thickness. The plates are pretreated with polyimide and rubbed to get homogeneous alignment of the molecules in the mesophase as described in chapter-I. The thickness of the cell is measured by using interferometric technique as described in chapter-I. The lock-in amplifier (LIA), (model PAR, 5302) supplies the sinusoidal voltage to the cell. A laser (He-Ne, λ=632.8nm) beam is passed through a polariser and made to be incident on the sample. The transmitted beam is passed through an analyser, which is crossed with respect to the polariser. A photodiode (PD1, model Centronics OSD-5) is used to measure the transmitted optical intensity. The stability of the laser intensity is monitored by another photodiode (PD2). A multimeter (MUL, model HP 3457A) measures the output voltages of the reference photodiode. The whole experiment is controlled by a computer using a suitable program.

The transmitted intensity of light beam through a uniaxial medium between two crossed polarisers whose optic axis is orthogonal to the propagation direction is given by

$$I_t = \frac{\sin^2 2\zeta}{2}(1-\cos\Delta\varphi) \tag{5.13}$$

where ζ is the azimuthal angle between the optic axis and the plane of polarisation of the incident light and $\Delta\varphi$ is the phase difference. If the difference between the D.C. signals measured at $\zeta = \pi/8$ radians and at zero azimuthal angle is I_0, using equation (5.13) we get,

$$I_0 = \frac{1}{4}(1-\cos\Delta\varphi). \tag{5.14}$$

When an A.C. electric field is applied to the cell the induced tilt angle also oscillates at the same frequency of the applied field (Fig.(5.6)). The oscillatory component of the transmitted intensity is given by

$$I_f = \sin 4\zeta\,(1-\cos\Delta\varphi)\delta\zeta\,. \tag{5.15}$$

In the geometry of the experiment $\zeta = \pi/8$ and $\delta\zeta = \theta$, which is the induced tilt angle. Hence

$$I_f = (1-\cos\Delta\varphi)\theta\,. \tag{5.16}$$

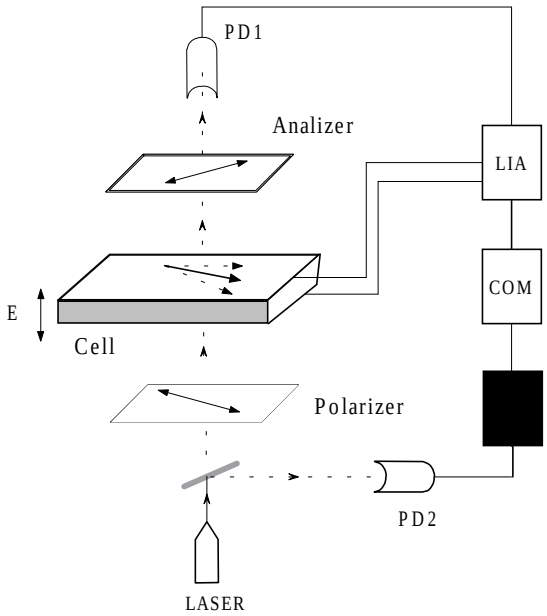

Figure 5.6: Schematic diagram of the experimental setup for the electroclinic measurement. Lock-in amplifier (LIA). Multimeter (MUL), Photodiodes (PD1, PD2).

Using equations (5.14) and (5.16) we get $\theta = I_f / 4I_0$. The measured electroclinic coefficient is given by

$$e = \theta / E_0 = I_f / 4I_0 E_0 . \qquad (5.17)$$

where E_0 is the amplitude of the applied electric field.

5.4 Results and Discussion

5.4.1 Helical Pitch in the Cholesteric Phase

The pitch in the cholesteric phase is measured at normal incidence using an Ocean Optics spectrometer (S2000) in the reflection mode. A block diagram of the relevant experimental setup is shown in Fig.(1.18) of chapter-I. The pitch values have been measured in a few mixtures as functions of temperature. A typical optical reflectivity spectrum is shown in Fig.(5.7). We notice the oscillations at the two sides of the reflection band which arise from the finite thickness of the sample [15].

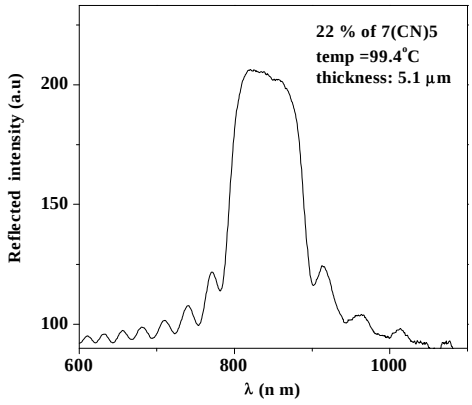

Figure 5.7: A typical reflection spectrum from cholesteric phase. The oscillations arise from the finite thickness of the sample [15].

In Fig.(5.8) the variations of the maximum of the reflection band (λ_0) are shown as functions of temperature for a few mixtures. We notice that λ_0 increases as the temperature is lowered in the cholesteric phase and it increases rappidly as the cholesteric to TGB_A transition temperature (T_{TGB_A-Ch}) is approached.

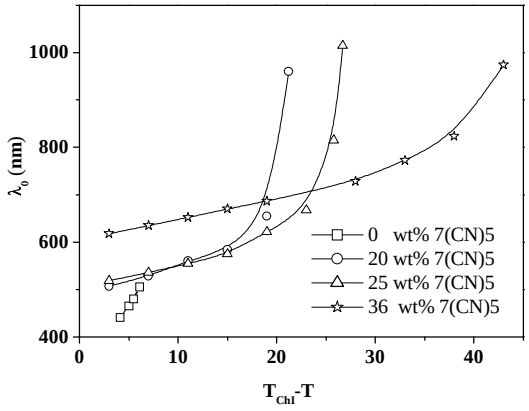

Figure 5.8: Variations of the maximum of the reflection band (λ_0) as functions of temperature for different concentration of 7(CN)5 in the mixtures. Continuous lines are drawn as guides to the eye.

The wavelength of the maximum of the reflection band, $\lambda_0 = \bar{n}P$ where $\bar{n}$ is the average refractive index with a value ≈1.5 for all the mixtures and P is the pitch of the helix. In Fig.(5.9), $1/P$ is plotted at (i) $4\ ^0$C below the isotropic to cholesteric transition

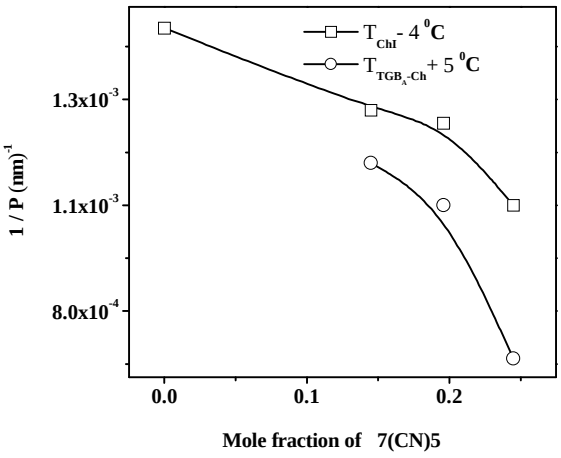

Figure 5.9: Variation of $1/P$ with mole fraction of 7(CN)5. The continuous lines are drawn as guides to the eye.

temperature ($T_{ChI} - 4^0$) and (ii) 5 ^{0}C above the TGB_A to cholesteric transition temperature ($T_{TGB_A-Ch} + 5^0$) respectively. In both the cases 1/*P*, which is a measure of the chiral strength, decreases with increasing concentration of 7(CN)5, as expected. We could not observe the reflection band in the TGB_A phase due to the limited wavelength range (~1100 *nm*) of the Ocean Optic spectrometer (model S2000).

5.4.2 Electroclinic Measurements

We have measured the electroclinic coefficient of a few mixtures as a function of temperature in the SmA phase. The same cell in which the pitch is measured is used for electroclinic measurements. The variation of a typical electroclinic signal (I_f) in the SmA phase is shown in Fig.(5.10).

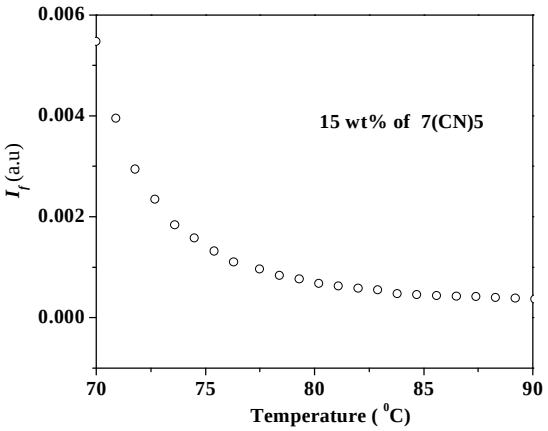

Figure 5.10: Variation of a typical electroclinic signal of the mixture of 15% wt of 7(CN)5. Cell thickness 5μm, applied voltage V_0 = 5V.

The calculated electroclinic coefficients for two mixtures are shown in Fig.(5.11) and in Fig.(5.12) as functions of temperature. A nonlinear least squares fitting procedure is used to fit the electroclinic coefficient with the inverse of (T-T_{AC}*) to get the ratio of the tilt elastic constant and the tilt-polarisation coupling constant i.e. (*a*/*k*) (see equation (5.13)). Using $k \approx 10^{-4}\ C/m^2$ typical for the low polarisation material [10], '*a*' is plotted as a function of concentration of 7(CN) 5 in Fig.(5.13). The Landau coefficient '*a*' is

proportional to the tilt elastic constant *D*. It is noticed from Fig.(5.12) that '*a*' and hence *D* decrease more than 4 times as the mole fraction of 7(CN)5 is increased from0 to 0.24. This means that $\kappa_2 (= \lambda_2 / \xi$,where $\lambda_2 = \sqrt{K_2 / D})$ roughly doubles in this range and increases further for the concentration at which the $UTGB_C$* phase is

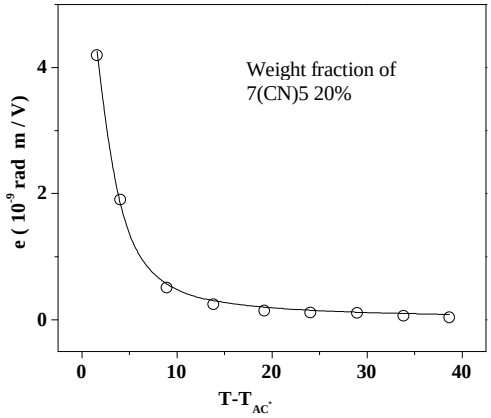

Figure 5.11: Variation of the electroclinic coefficient with temperature for the mixture with 20 wt% of 7(CN)5. Circles: experimental data. Continuous line is a fit to the functional form of $e = k / a(T - T_{AC^*})$.

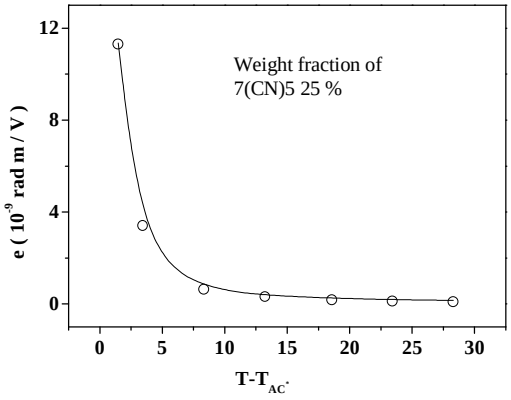

Figure 5.12: Variation of the electroclinic coefficient with temperature for the mixture with 25 wt % of 7(CN)5. Circles: experimental data. Continuous line is a fit to the functional form of $e = k / a(T - T_{AC^*})$.

induced. The enhancement of the type-II character accounts for the increased temperature range of TGB_A phase with the concentration of 7(CN)5 (see Fig.(5.3)).

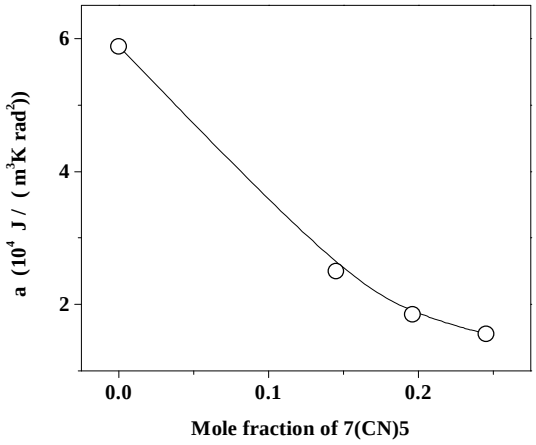

Figure 5.13: The Landau coefficient '*a*' proportional to the tilt elastic constant *D* shown as a function of mole fraction of 7(CN)5. The continuous line is a guide to the eye.

5.4.3 Effect of a Strong Electric Field on the TGB_A Phase

We studied the influence of a low frequency electric field along the helix axis of the TGB_A phase on its texture. In the lower temperature part of the TGB_A phase the mixtures with 20wt% and 25wt% of 7(CN)5 show an *irreversible* TGB_A to SmA transition under the action of a large (~10 V /μm) low frequency (10Hz) field. A similar effect was reported by Shao *et al* [16]. The change of texture is shown in Fig.(5.13). The Joule heating of the system due to the application of field would have led to a transition to the cholesteric phase as it occurs above the temperature range of TGB_A phase. The origin of the field induced unwinding of the TGB_A helix in these systems is not yet understood. On the other hand, it is interesting that in the mixtures exhibiting the $UTGB_C$* phase, a *reversible* transition to SmC* phase is observed under a low frequency field (50Hz ; 13V/μm).

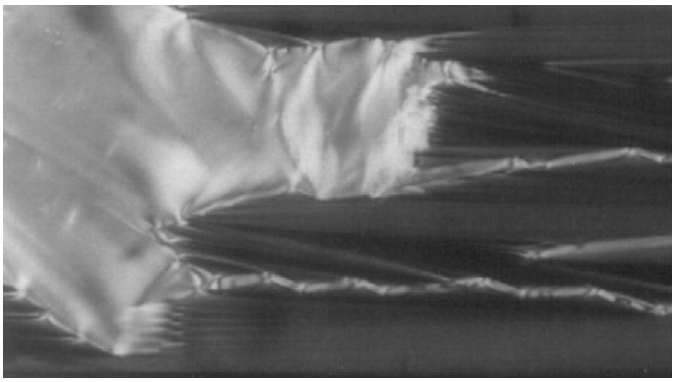

Figure 5.14: Field induced transition from the TGB_A phase (bright region) into the SmA phase in the mixture with 25 wt% of 7(CN)5 at 108.5 ^{0}C. Crossed polarisers (X 500).

5.4.4 Freestanding Films

We have studied freely suspended films of mixtures, which exhibit the TGB_A and $UTGB_C$* phases. The liquid crystalline films are suspended across a hole drilled in a glass plate. The observations reported here are made on mixtures having about 36wt % of 7(CN)5. At a temperature corresponding to the occurrence of the TGB_A phase the structure is unwound in the central flat part of the film. The homeotropically aligned smectic layers appeared dark between crossed polarisers. Three distinct regions could be distinguished in the meniscus region. In the thicker part of the meniscus, close to the periphery of the hole, filaments which are characteristic of the TGB_A liquid crystal subjected to homeotropic boundary conditions, could be observed (Fig.(5.15)). The director rotates by π radians across the filament, whose width is $P/2$, where P is the pitch of the TGB helix. The filaments are oriented parallel to the edge of the hole. The width is nearly independent of the local thickness. Some filaments sharply turn by 90^0 near the thinnest part in which they are seen and extend along the radial direction (Fig.(5.15)). A *new* type of periodic structure is seen in the intermediate thickness region of the meniscus and is found to consist of alternate bright and dark stripes between crossed polarisers (see Fig.(5.15)). The radial stripes (RS) have a low contrast in comparison to the filaments, which are very bright even when oriented along the

radial direction. On rotation of the crossed polarisers, the width of the dark region of the RS decreases when the polariser axis is at 45^0 to the radial direction.

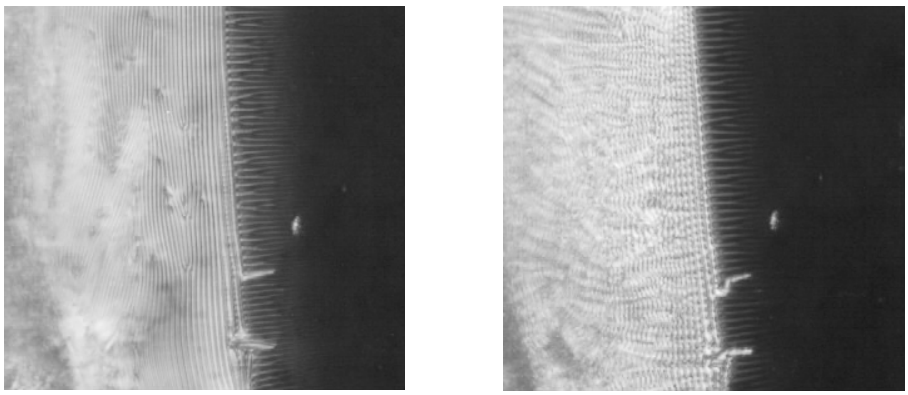

(a) (b)

Figure 5.15: (a) (Left) Meniscus region of the free standing film of the mixture with 36 wt% of 7(CN)5 in the TGB_A phase at 59.8 ^{0}C. Crossed polarisers (X 400). The central flat part is at the right extreme, the radial structure is seen in the central part of the meniscus and the filaments are in the thickest part of the meniscus. (b) Sample in the $UTGB_C^*$ phase at 57.4 ^{0}C. Note the undulation of the filaments.

Careful observations show that the bright stripes do not have a uniform intensity along their length but are marked by narrow bands of lower intensity, which are orthogonal to the radial direction. The average spatial periodicity of the radial stripes increases with film thickness, which is brought about by the introduction of edge dislocations (Fig.(5.15)). The thinnest part of the meniscus region appears completely dark between crossed polarisers. The contrast of RS becomes lower as the thickness of the meniscus region is decreased. It is not clear whether the spatial periodicity of the radial structure in the thinnest part is too small to be resolved by the microscope.

When the sample is cooled into the $UTGB_C^*$ phase the filaments in the thicker part of the meniscus are undulated (Fig.(5.15)) as expected [7]. The periodic RS structure in the intermediate region however remains intact.

Somewhat similar regularly spaced radial domains have been observed in the meniscus region of thin freestanding films of a nonchiral SmC sample [17]. This has been attributed to surface polarisation, which gives rise to a periodic splay deformation of the C-director. When such a sample is rotated between crossed polarisers the relative positions of the bright and dark domains can be expected to depend on the orientation of the polariser axis with respect to the radial direction. In the TGB_A sample studied by us there is no molecular tilt in the layers. Further, the positions of the bright and dark stripes of the periodic structure do not shift under a rotation of crossed polarisers. The origin of the RS observed by us, cannot be the one described above.

Recent observations with a confocal microscope, on a free-standing film of the same TGB sample used by us have shown evidence for the occurrence of edge dislocations with large Burgers vectors in the smectic layers of the meniscus region [18]. The spacing between the dislocations decreases towards the thicker part of the meniscus. The sharp bands orthogonal to the radial direction of the stripes that we described earlier appear to correspond to these edge dislocations. Recent studies on the meniscus region of free-standing films of type-I smectic liquid crystals (like alkyl cyanobiphenyls) have shown that the edge dislocations have Burgers vectors equal to single layer spacing in the thinnest region while larger Burgers vectors occur in the thicker parts. The latter go over to rows of focal conics [19]. On the other hand studies on swollen lamellar phases in a lyotropic system taken between a slide and a convex lens have shown that the Burgers vectors of edge dislocations are large, and increase from ten to thirty as the sample thickness is increased [20]. Our type-II system appears to be similar to the latter system.

A possible arrangement of smectic layers in the meniscus region of our system is shown in Fig.(5.16). As the surface tension of smectic layers is ≈ 30 dyne / cm [18], we expect that the layers near the surface have a smooth profile. The occurrence of edge dislocations with large Burgers vectors then leads to regions with a large tensile strain (Fig.(5.16)).

It is known that beyond a tensile strain $\approx 2\pi\lambda_1/d$, where λ_1 is the splay penetration length given by $\sqrt{(K_1/B)}$, K_1 being the splay elastic constant and B the compression constant of the layers and d the layer spacing, the layers can undulate to fill space [1]. In

the intermediate thickness region, such an instability can generate the RS seen in the experiments. The periodicity of the structure would depend on the local thickness [1] as seen in the experiment. The undulation instability is usually metastable and gives rise to

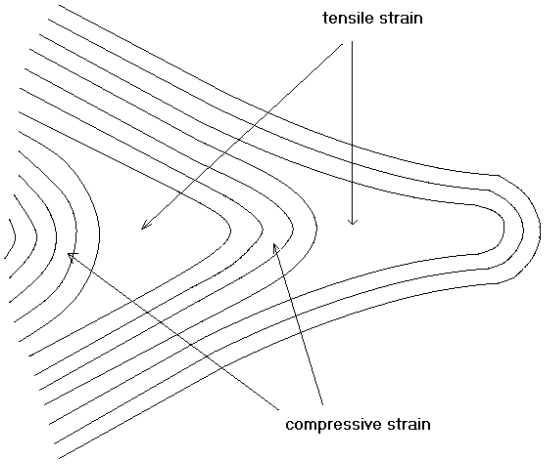

Figure 5.16: Schematic diagram of the arrangement of smectic layers in the meniscus region. The undulation of the layers is expected to take place in the region with tensile strain, along a direction perpendicular to the plane of the paper, in which the local thickness is constant.

other structures over a period of time [1]. On the other hand, the RS structure is indeed stable and is better formed if the sample temperature is held constant for several hours. A detailed theoretical analysis to understand this new feature is desirable.

We have also made observations on an open drop of the liquid crystal taken on a glass plate treated for homeotropic alignment. The drop has a flattened hemispherical shape. As in the freestanding film there was a decrease in thickness on moving towards the edge of the drop. The periodic radial structure was obtained in this case also with its spacing decreasing towards the periphery of the drop.

5.5 Conclusions

We have demonstrated that the type-II character is enhanced in the mixtures studied by us by increasing the concentration of the nonchiral component, which in turn enlarges the temperature range of TGB phases. We have also found an unusual radial stripe texture in an intermediate thickness region of the meniscus in freestanding films of the type-II material. We argue that these are generated by an undulation instability of the smectic layers in the regions of high tensile strain associated with edge dislocations with large Burgers vectors. Though the swollen lamellar phase also exhibits edge dislocations with large Burgers vectors, the orthogonal periodic stripes have not been reported in that case. Our system has a decidedly type-II character and the RS structure appears to be associated with this feature.

References

[1] P. G. De Gennes, and J. Prost, "The physics of liquid crystals.," 2nd ed. (Clarendon Press, Oxford, 1995).

[2] S. R. Renn, and T. C. Lubensky, " Abrikosov dislocation lattice in a model of the cholesteric to smectic-A transition.," Phys. Rev. A, **38**, 2132 (1988).

[3] J. W. Goodby, M. A. Waugh, S. M. Stein, E., Chin, R. Pindak and J. S. Patel, " Characterization of a new helical smectic liquid crystal.," Nature **337**, 449 (1989).

[4] L. Navailles, B. Pansu, L. G. Talini and H. T. Nguyen, "Structural study of commensurate TGB_A and presumed chiral line liquid phase.," Phys. Rev. Lett. **81**, 4168 (1998).

[5] P. M. Chaikin and T. C. Lubensky, "Principles of condensed matter physics.," Cambridge University press, Cambridge (1995).

[6] L. Navailles, R. Pindak, P. Barois, and H. T. Hguyen, “Structural study of the smectic –C twist grain boundary phase.,” Phys. Rev. Lett. **74**, 5224 (1995).

[7] P. A. Pramod, R. Pratibha, and N. V. Madhusudana, “A three dimensionally modulated structure in a chiral smectic-C liquid crystal.,” Current Science **73**, 9 (1997).

[8] P. A. Pramod, R. Pratibha, Sobha. R. Warrier and N. V. Madhusudana, “Experimental studies on the undulated twist grain boundary-C* liquid crystal.,” Ferroelectrics **244**, 31 (2000).

[9] P. Wilson, S. Cowling and D. Lacey, “Synthesis and evaluation of novel selenophene - and thiophene –containing liquid crystalline materials exhibiting TGBC* phases.,” paper presented at the 8th International Conference on Ferroelectric Liquid Crystals (2001).

[10] R. B. Meyer, L. Liebert, L. Strzelecki and P. Keller, “Ferroelectric liquid crystals.,” J. Phys. Lett. (Paris) 3**6**, L69 (1975).

[11] S. Garoff and R. B. Meyer, “Electroclinic effect at the A-C phase change in a chiral smectic liquid crystal.,” Phys. Rev Lett. **38**, 848 (1977); S. Garoff and R. B. Meyer, “Electroclinic effect at the A-C phase change in a chiral smectic liquid crystal.,” Phys. Rev. A, **19**, 338 (1979).

[12] H. P. Padmini, R. Pratibha, N.V. Madhusudana and B. Shivkumar, “ Electroclinic response of some ferroelectric liquid crystals.,” Liquid Crystals, **14**, 435 (1993).

[13] C. Bahr and G. Heppke, “Behavior of the electroclinic effect in homologous series of ferroelectric liquid crystals.,” Phys. Chem. **95**, 761 (1991).

[14] G. Andersson, I Dahl, W. Kuczynski, S. T. Lagerwall, K. Skarp and B. Stebler, “The soft-mode ferroelectric effect.,” Ferroelectrics, **84**, 285 (1988).

[15] S. Chardrasekhar, “Liquid Crystals.,” 2nd ed. (Cambridge University Press,1992).

[16] R. Shao, J. Pang, N.A.. Clark, J.A . Rego, M. D. Walba, “Electric field induced transitions from TGB_A^* and TGB_C^* to smectic A^* and C^* states.,” Ferroelectrics, **147**, 255 (1993).

[17] R. B. Meyer and P.S. Pershan, “Surface polarity induced domains inliquid crystals.,” Solid State Comm. **13**, 989 (1973).

[18] I. I. Smalyukh, R. Pratibha, O. D. Lavrentovich and N. V. Madhusudana (Liq. Cryst. in press).

[19] F. Picano, R. Holyst and P. Oswald, “Coupling between meniscus and smectic-A film: circular and catenoid profiles, induced stress, and dislocation dynamic.,” Phys. Rev. E, **62**, 3747 (2000).

[20] F. Nallet and J. Prost, “ Edge dislocation arrays in swollen lamellar phases.,” Europhys. Lett. **4**, 307 (1987).